# A COMPARISON OF GPS CLOCK MODELS FOR THE NEXT GENERATION GPS SYSTEM TIMESCALE

**Michael J. Coleman[1] and Ken Senior**
**U.S. Naval Research Laboratory**
**4555 Overlook Avenue, SW**
**Washington, DC 20375**
**TEL: 01 202 767 4273[1]**

**Abstract**

***The on–orbit GPS satellite clock signals demonstrate significant periodic fluctuations for periods of 2.003 and 4.006 cycles/day. A timescale algorithm which includes the on–orbit GPS clocks should account for these periodic variations in order to mitigate their influence on the timescale. This is accomplished in a Kalman filter by introducing the periodics as independent states which evolve in a discrete–time algorithm alongside four other clock dynamic states. However, there is some freedom in the choice of how these harmonic states are coupled to the other states depending on the application at hand. A typical model of a clock's dynamics is a four state clock model, including the phase of the clock, its first derivative (frequency) and its second derivative (drift), each perturbed by an independent random walk; one additional phase state is also included in order to model a pure white phase noise. Four additional states are joined with the typical clock states in order to accommodate the periodic processes, where each of the four harmonic states are also perturbed by stochastic noises of some type (e.g., random walks) in order to account for any random change in the harmonic amplitude or phase over time.***

***In general, a Kalman filter will grow in complexity with the number of states and the number of non–trivial correlations between them. Since the process noise covariance matrix will have off–diagonal entries for the discrete model, including those between the typical clock dynamic states and the harmonic states, reducing unnecessary correlations can lead to reduced complexity and improved processing time for the filter implementation. If the process noise covariance between the harmonic states and the clock dynamic states are small, then a filter algorithm that neglects these small cross–correlations (and hence simplifies the state covariance matrix) is preferable and can be exploited to reduce processing time.***

***This work investigates the performance of the fully coupled model in comparison with the reduced covariance model, where performance is measured in terms of both timescale stability, model accuracy, and processing time. The benefits and costs of coupling the harmonics only to the phase state versus coupling them fully to the drift and frequency states is also investigated.***

## INTRODUCTION

Good filter performance for a timescale is reliant on an accurate model of the clocks' behaviors. As GPS clocks have continued to improve with each new generation, so has our ability to measure (or estimate) their signals remotely using techniques such as geodetic time transfer. Increased global density of GPS tracking stations, the utilization of geodetic quality receivers that can track multiple satellites on both frequencies, as well as utilization of integrated Doppler observations have led to the routine comparison of remote clocks at the centimeter level globally as evidenced, for example, in the products of the International GNSS Service. Throughout this work, the term "clock" is meant to encompass all non–dispersive bias–like effects on a

given clock signal. In the case of satellite clocks, this means not only the contribution from the active atomic physics package on board the satellite but also any other bias–like effects from other elements in the transmit chain leading up to transmission of the signal at the antenna. For ground station clocks, this includes not only the frequency reference used by the GPS receiver but also all other bias–like effects in the GPS receive chain.

Using data from the IGS the authors in **[1]** determined that the GPS constellation clocks are subject to significant harmonic variations at periods of $n \times (2.0029 \pm 0.0005)$ cycles per day for $n \in \{1, 2, 3, 4\}$ with lesser amplitudes for $n = 3$ and $n = 4$, specifically. Any timescale which utilizes the GPS satellite clocks should therefore compensate the harmonic variations, particularly for $n = 1$ and $n = 2$. This paper compares several similar approaches to handling these two periodics in the context of Kalman filtering, each with subtle model differences as well as different impacts on the speed of computation.

In order to closely model the expected configuration of the GPS operational control segment network of clocks, we assume in this analysis a collection of 41 clocks: 15 ground high performance commercial cesium clocks, 24 GPS constellation clocks with performance similar to the Block IIF performances and 2 commercial active masers. The goal is to generate a timescale from these 41 clocks utilizing three different approaches to modeling the harmonic variations. In each of the three approaches the same timescale constraints will be added to the system so that only the particular handling of the harmonic variations differs in the comparisons.

The first section of this paper will introduce the base clock model that is employed for all of the clocks in this analysis. A four state model is chosen in order to address an additional white noise process in the clock's phase. The clock dynamics are introduced in a continuous version of the model. The discrete model is obtained by standard techniques that can be found in **[2]**. The variance of the stochastic white noise sequences is defined as an input parameter, and derivations of key covariance matrices are also presented. The base clock model is all that is required to analyze the cesium clocks and masers since no other known factors are significantly important.

Additional states necessary to model the harmonic variations for the GPS clocks are presented in the second section. Within this section are three different models of the clock periodic states: the first adds the states to only the phase state without any stochastic correlation between the stochastics driving the harmonics and the stochastics driving the base model; a second provides for full correlation between the harmonic stochastics and the base model stochastics but results in higher algorithm complexity; and a third model couples the harmonics to all clock states and stochastically correlates them entirely. The structure of the matrices involved in the algorithm are derived for each model in this section. A large diagram is also shown to exhibit how each noise traverses the clock's states and thereby how each affects the clock signal output.

The modeling constraints used to generate the ensemble is presented in the third section. Also, the standard Kalman filter process that is used to filter measurements for the ensemble is shown for completeness. Details of the filter and the matrices that are used in this case are derived. There is also an explanation of the filter components which contribute most to the computation time of the algorithm. A key element of this study is to identify the algorithm speed that is sacrificed when greater noise correlations are made. The fourth section closes the analysis with results of each of these models applied to the filter. A study of the complexity bestowed upon the filter by each model is presented. A comparison of the clock deviations, timescale deviations and filter run times allow us to determine which model may best support a timescale filter for the ensemble involving on–board GPS clocks.

### Notational Conventions

Bracketed superscripting/subscripting will always denote quantities pertaining to individual clock members. For example, $x_1^{[i]}$ denotes the phase of clock $i$ relative to a perfect clock. When the continuous–time model is discussed, we will use the variable $t$ to denote the independent "perfect time" measurement. The majority of this report, however, revolves around a discrete model. We will denote by $t_k$ the discrete epoch of the timescale from a clock common to all the measurements and estimates. Variations in the difference $\tau := t_k - t_{k-1}$ are neglected as insignificant. In cases where the quantity of interest is dependent on only $\tau$, the epoch variable $t_k$ will be dropped to simplify notation.

Subscripts exhibited on bold matrix variables (as in $\mathbf{A}_{m,n}$) are used to denote the size of the matrix. For example, $\mathbf{A}_{4,3N}$ would indicate that matrix $\mathbf{A}$ has size $4 \times 3N$. If only one index is listed in the subscript, then the matrix is square. When subscripts appear on matrix variables of normal italic type (as in $A_{m,n}$), then the expression $A_{m,n}$ represents the entry in position $(m, n)$ of matrix $\mathbf{A}$. The matrices $\mathbf{0}_{m,n}$ and $\mathbf{0}_n$ are the zero matrices of sizes $m \times n$ and $n \times n$, respectively. We denote the size $n \times n$ identity matrix by the symbol $\mathbf{I}_n$.

## BASE CLOCK MODEL

Two–state perfect integrators were first suggested to model the error of clocks by Jones and Tryon during the early 1980s **[3]**. Phase and frequency were the states used in the two–state model. By 1982, the inclusion of a linear clock drift term brought about three state clock models, necessary particularly to model the drift of masers and rubidium clocks **[4]**. The four state model has since been used to model the behavior of most clocks. See **[5]**, for example. An additional phase state with its own white noise process is the fourth state that sets this model apart from the two and three state versions. In this paper, cesium clocks and masers will be modeled using the four state clock model. The primary focus, however, is the set of GPS constellation clocks. These will require additional states to handle their periodic variations. Extensions of the model for the GPS clocks will be discussed in the next section; this section handles only the four state clock model.

### Continuous Version

The four states of this model are the clock's phase, derivative of phase (frequency), second derivative of phase (drift), and an additional phase state. Independent integrated white noise components (random walks) are added to each of the deterministic states of drift, frequency and phase. The additional phase state is equal to the clock's phase plus an additional non–integrated white noise. A state vector $\mathbf{x}$ and corresponding noise input vector $\mathbf{u}$ contain the variables of the states and input noises for the clock. These are shown below to identify the nomenclature for the states and noise components.

$$\mathbf{x}(t) = \begin{bmatrix} x_1(t) \\ x_2(t) \\ x_3(t) \\ x_4(t) \end{bmatrix} \begin{matrix} \text{Perturbed Phase} \\ \text{Phase} \\ \text{Frequency} \\ \text{Drift} \end{matrix} \qquad \begin{matrix} \text{White Phase Noise} \\ \text{Random Walk Phase Noise} \\ \text{Random Walk Frequency Noise} \\ \text{Random Walk Drift Noise} \end{matrix} \begin{bmatrix} u_1(t) \\ u_2(t) \\ u_3(t) \\ u_4(t) \end{bmatrix} = \mathbf{u}(t)$$

A diagram of the dynamics for these four clock states and the corresponding input white noise sequences is shown below in Figure 1. In this figure, one can see how the noises are integrated to become random walks or random runs upon contribution to the output clock signal.

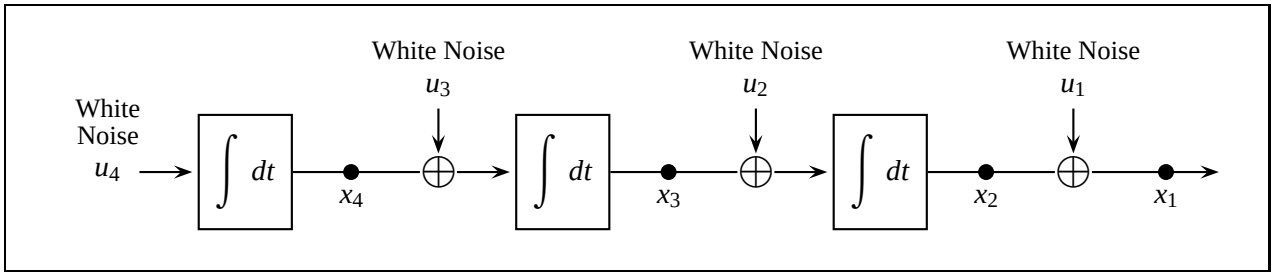


Figure 1. Model of a clock's four states and independent input white noises.

This model is analogous to an acceleration model where drift, frequency and phase are the analogs of acceleration, velocity and displacement. With this similarity drawn, the systems of differential equations modeling the clock depicted in Figure 1 is clearly

$$\mathbf{C}\frac{d\mathbf{x}}{dt} = \mathbf{F}\,\mathbf{x}(t) + \mathbf{u}(t) \tag{1}$$

where $t$ is an independent "perfect time" variable and the coefficient matrices are

$$\mathbf{C} = \begin{bmatrix} 0 & 0 & 0 & 0 \\ 0 & 1 & 0 & 0 \\ 0 & 0 & 1 & 0 \\ 0 & 0 & 0 & 1 \end{bmatrix} \quad \text{and} \quad \mathbf{F} = \begin{bmatrix} 1 & -1 & 0 & 0 \\ 0 & 0 & 1 & 0 \\ 0 & 0 & 0 & 1 \\ 0 & 0 & 0 & 0 \end{bmatrix}.$$

Each of the noise inputs are white noise sequences which we will assume to have mean zero and variances defined by $E\left[\,\mathbf{u}(t)\mathbf{u}^T(t')\,\right] = \mathbf{S}\,\delta_0(t-t')$ where $\mathbf{S} = \text{Diag}[\,S_1\,,\,S_2\,,\,S_3\,,\,S_4\,]$ and $\delta(x)$ is the standard Dirac delta function.

## Discrete Version

An equivalent discrete model can be developed by first setting a distribution of evenly spaced time epochs at intervals of $\tau$; see Figure 2. These epochs are enumerated with the index $k$. An implementation of this model involves estimating the clock states at each of these epochs. One can calculate the state vector at time epoch $t_{k+1}$ based entirely on the state values at the epoch $t_k$ and the white noise process by

$$\mathbf{x}(t_{k+1}) = \Phi_k(t_{k+1})\mathbf{x}(t_k) + \mathbf{G}\,\mathbf{s}(t_k) \tag{2}$$

where the transition matrix that propagates the state from $t_k$ to $t_{k+1}$ is given by

$$\Phi_k(t_{k+1}) = \begin{bmatrix} 0 & 1 & t_{k+1}-t_k & (t_{k+1}-t_k)^2/2 \\ & 1 & t_{k+1}-t_k & (t_{k+1}-t_k)^2/2 \\ & & 1 & t_{k+1}-t_k \\ & & & 1 \end{bmatrix} = \begin{bmatrix} 0 & 1 & \tau & \tau^2/2 \\ & 1 & \tau & \tau^2/2 \\ & & 1 & \tau \\ & & & 1 \end{bmatrix}.$$

The matrix $\mathbf{G}$ is called the process noise pre–multiplier. It serves to add both the random walk phase noise and the white phase noise to the additional phase state. Note that the phase state whose derivative is set to frequency does not have an additional white noise process. The process noise pre–multiplier and random

noise inputs to the system, in evolving discretely from $t_k$ to $t_{k+1}$, are

$$\mathbf{G} := \begin{bmatrix} 1 & 1 & 0 & 0 \\ 0 & 1 & 0 & 0 \\ 0 & 0 & 1 & 0 \\ 0 & 0 & 0 & 1 \end{bmatrix} \qquad \text{and} \qquad \mathbf{s}(t_k) := \mathbf{G}^{-1} \int_{t_k}^{t_{k+1}} \Phi_k(\xi)\mathbf{u}(\xi)\, d\xi. \tag{3}$$

From this point forward, we define the notation $\mathbf{x}_k := \mathbf{x}(t_k)$ and $\mathbf{s}_k := \mathbf{x}(t_k)$ for simplicity. Both of these conventions will appear later, depending on context.

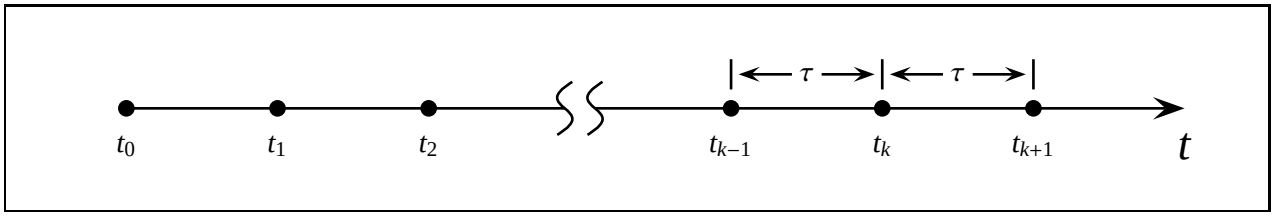


Figure 2. Discrete enumerated epochs on a continuous time axis.

From Equation (3) and the assumption of the noise expectation in the continuous model, one can derive

$$E\,[\,\mathbf{G}\mathbf{s}_k\,] \;=\; \int_{t_k}^{t_{k+1}} \Phi_k(\xi) E\,[\,\mathbf{u}(\xi)\,]\, d\xi \;=\; \mathbf{0}_{4,1}.$$

Since $\mathbf{G}$ is a constant invertible matrix, the mean of each discrete noise statistic must be 0. Applying the definition of $\mathbf{s}_k$ in Equation (3), the covariance matrix associated with the discrete white noise statistics is

$$\mathbf{G}\,\mathbf{Q}_k\mathbf{G}^T \;=\; \int_{t_k}^{t_{k+1}} \int_{t_k}^{t_{k+1}} \Phi_k(\xi)\,\mathbf{S}\,\Phi_k^T(\eta)\,\delta_0(\xi-\eta)\,d\eta\,d\xi. \tag{4}$$

From this, and recalling that $\tau = t_{k+1} - t_k$, the $\mathbf{Q}_k$ matrix may be explicitly calculated as

$$\mathbf{Q}_k \;=\; \begin{bmatrix} S_1 f_h & 0 & 0 & 0 \\ 0 & S_2\tau + S_3\frac{\tau^3}{3} + S_4\frac{\tau^5}{20} & S_3\frac{\tau^2}{2} + S_4\frac{\tau^4}{8} & S_4\frac{\tau^3}{6} \\ 0 & S_3\frac{\tau^2}{2} + S_4\frac{\tau^4}{8} & S_3\tau + S_4\frac{\tau^3}{3} & S_4\frac{\tau^2}{2} \\ 0 & S_4\frac{\tau^3}{6} & S_4\frac{\tau^2}{2} & S_4\tau \end{bmatrix} \tag{5}$$

where $f_h$ is a high frequency cut–off to limit the bandwidth of the white phase variance. The off–diagonal entries of $\mathbf{Q}_k$ can be specified either from manufacturer's specification or from Hadamard analysis of the clock signal **[6]**. It is worth noting that the epoch number $k$ is absent from the structure of the matrices $\Phi_k$, $\mathbf{G}$ and $\mathbf{Q}_k$. This is a result of the stationary nature of the white noise processes. Often, the epoch number subscript may be dropped when it is clearly superfluous. See **[2]** for further details on the development of the discrete time model.

## GPS CLOCK MODELS

The clocks aboard the GPS constellation satellites exhibit periodic perturbations in the measurements observed. While the precise source of these effects is not known, their mathematical nature has been identified as sinusoidal perturbations with periods of 2.003 and 4.006 cycles/day **[1]**.

Since there are two periodics that affect a GPS clock, we expand the base model of the last section by adding four additional states. It is necessary to add two states per periodic since a sinusoid is uniquely determined by a phase and an amplitude. Three models will be presented and the only difference between them will be the method by which these periodic states are coupled and correlated to the clock dynamic states. The coupling of the periodic variables is described in the diagram of Figure 3. Note that in Model I, the harmonics are added directly to the output phase of the clock to directly simulate the intrusion of the periodic in the clock signal. Model II injects the oscillating harmonic to both phase states in order to reconcile the two phase states as equivalent up to one white noise process. Model III couples all the clock dynamic states to the periodics.

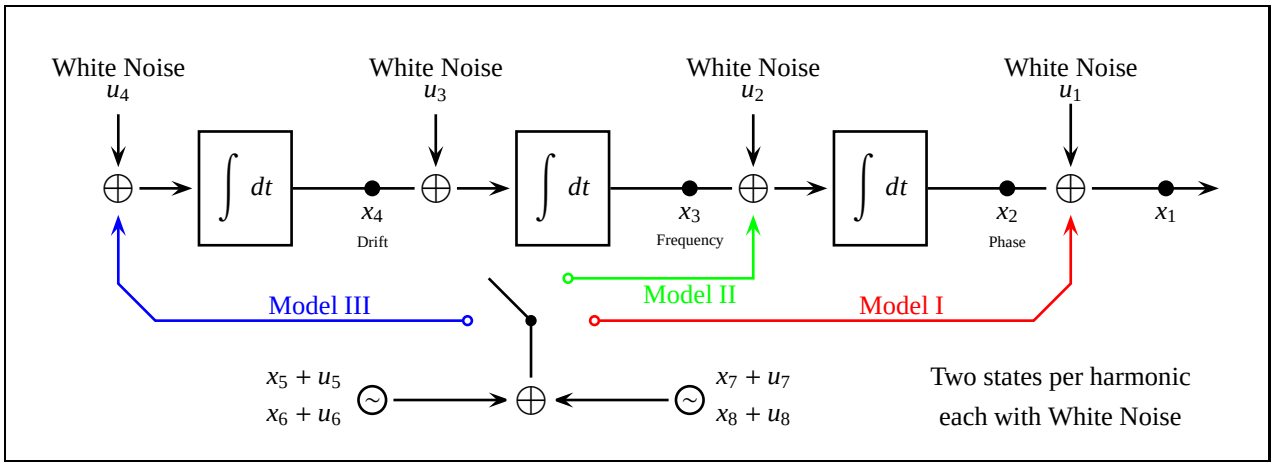


Figure 3. Clock model with fixed period harmonics added in one of three ways.

For GPS clocks, the presence of harmonics requires an expansion of the state and noise vectors. Since there must be two states per periodic, these vector expand to the following.

$$\mathbf{x} = [\, x_1,\, x_2,\, x_3,\, x_4,\, x_5,\, x_6,\, x_7,\, x_8 \,],$$
$$\mathbf{u} = [\, u_1,\, u_2,\, u_3,\, u_4,\, u_5,\, u_6,\, u_7,\, u_8 \,].$$

With these expanded vectors comes the expanded covariance matrix. As with the base model, this covariance matrix is equal to a delta function multiplied by the matrix

$$\mathbf{S} = \mathrm{Diag}[\, S_1\,,\, S_2\,,\, S_3\,,\, S_4\,,\, S_h\,,\, S_h\,,\, S_h\,,\, S_h\,].$$

For simplicity, it is assumed that the harmonic states have the same level of noise. In other words,

$$E\left[u_5^2\right] = E\left[u_6^2\right] = E\left[u_7^2\right] = E\left[u_8^2\right] = S_h. \tag{6}$$

Although the periods of the sinusoids are fixed throughout this paper, the model is designed to accept two periodic influences of any period. Therefore, define the variables $\omega_1$ and $\omega_2$ to be the frequencies of the sinusoids mentioned in cycles/day. For this paper, it will be the case that $\omega_1 = 2.003$ and $\omega_2 = 4.006$. Furthermore, define the dimensionless versions of these frequencies

$$\nu_1 = 2\pi\omega_1 \qquad \text{and} \qquad \nu_2 = 2\pi\omega_2.$$

## MODEL I

The first model entails the simplest computational introduction of the fixed periodic influences. We simply add two fixed period harmonic oscillations to the phase state $x_1$ and weight them with the four harmonic state variables. Hence, the deterministic component of the phase state takes the form

$$x_1 = x_2 + \tau x_3 + \tfrac{\tau^2}{2} x_4 + x_5 \cos(\nu_1 t_k) + x_6 \sin(\nu_1 t_k) + x_7 \cos(\nu_2 t_k) + x_8 \sin(\nu_2 t_k).$$

Note that the harmonic variables are used as weights on the fixed period sinusoidal functions. This allows the filter to adjust the weights such that the amplitude and phase of the two harmonics are attained to correspond to those realized in the GPS clock measurements.

Since the harmonic effects are assumed to influence the clock and be completely unaffected by the clock states, we presume a total decorrelation of the harmonics and clock states. The continuous clock model for this case will therefore involve a periodic forcing as a delta function at each epoch. The differential model will be the same as in Equation (1), namely

$$\begin{bmatrix} \mathbf{C} & \mathbf{0}_4 \\ \mathbf{0}_4 & \mathbf{I}_4 \end{bmatrix} \frac{d\mathbf{x}}{dt} = \begin{bmatrix} \mathbf{F} & \mathbf{0}_4 \\ \mathbf{0}_4 & \mathbf{I}_4 \end{bmatrix} \mathbf{x}(t) + \mathbf{u}(t) \tag{7}$$

where the coefficient matrices are simply expansions of those presented in the base model. Upon integration (or use of an inverse Laplace Transform), one obtains a familiar transition matrix. The sinusoidal entries in the top row are added to the transition matrix to incorporate the harmonics into the $x_1$ phase state. The discrete model therefore has the form

$$\mathbf{x}_{k+1} = (\,\Phi_{\mathrm{I}} + \mathbf{M}_k\,)\mathbf{x}_k + \mathbf{G}_{\mathrm{I}}\mathbf{s}_k$$

where

$$\Phi_{\mathrm{I}} = \begin{bmatrix} \Phi & \mathbf{0}_4 \\ \mathbf{0}_4 & \mathbf{I}_4 \end{bmatrix} \qquad \text{and} \qquad \mathbf{G}_{\mathrm{I}} = \begin{bmatrix} \mathbf{G} & \mathbf{0}_4 \\ \mathbf{0}_4 & \mathbf{I}_4 \end{bmatrix}.$$

Also,

$$\mathbf{M}_k = \begin{bmatrix} \mathbf{0}_{1,4} & \cos(\nu_1 t_k) & \sin(\nu_1 t_k) & \cos(\nu_2 t_k) & \sin(\nu_2 t_k) \\ \mathbf{0}_{7,4} & \mathbf{0}_{7,1} & \mathbf{0}_{7,1} & \mathbf{0}_{7,1} & \mathbf{0}_{7,1} \end{bmatrix}.$$

In this simplified model, we assume no correlation between the harmonic states and the clock's phase. The intent of adding the harmonics in this fashion is to account for the superimposed undulations in the phase via fairly well–determined periodic influence. The reason for adding the periodics as states with stochastic processes is to give the filter stochastic flexibility to update the states should there be a change in the periodics. A purely deterministic periodic would be unaccommodating to any measurement changes or other such numerical inconsistencies. We therefore take the covariances of the harmonic states to be zero

and obtain the error covariance matrix in the same manner as in Equation (4):

$$E\left[\,\mathbf{G}_{\mathrm{I}}\,\mathbf{s}_k\mathbf{s}_k^T\mathbf{G}_{\mathrm{I}}^T\,\right] \;=\; \int_{t_k}^{t_{k+1}} \Phi_{\mathrm{I}}\mathbf{S}\,\Phi_{\mathrm{I}}^T\,d\tau \;=\; \mathbf{G}_{\mathrm{I}}\begin{bmatrix}\mathbf{Q}_k & \mathbf{0}_4\\ \mathbf{0}_4 & \tau S_h\mathbf{I}_4\end{bmatrix}\mathbf{G}_{\mathrm{I}}^T.$$

## MODEL II

For Model II, the periodic states are treated as oscillating variables themselves, rather than as weights to fixed trigonometric functions. The two most crucial differences between this and Model I are: the periodics are added into both phase states; and, the covariances between the clock and periodic states are not neglected. By allowing this stochastic connection, the error covariance matrix becomes inherently more complicated and therefore increases the computational complexity of the Kalman update routine.

The continuous model is again of the form in Equation (1). The coefficient matrix, however, differs substantially. For Model II, we have

$$\begin{bmatrix}\mathbf{C} & \mathbf{0}_4\\ \mathbf{0}_4 & \mathbf{I}_4\end{bmatrix}\frac{d\mathbf{x}}{dt} = \begin{bmatrix}
1 & -1 & 0 & 0 & & & & \\
0 & 0 & 1 & 0 & 1 & 0 & 1 & 0\\
0 & 0 & 0 & 1 & & & & \\
0 & 0 & 0 & 0 & & & & \\
 & & & & 0 & \nu_1 & & \\
 & & & & -\nu_1 & 0 & & \\
 & & & & & & 0 & \nu_2\\
 & & & & & & -\nu_2 & 0
\end{bmatrix}\mathbf{x}(t) + \mathbf{u}(t). \tag{8}$$

The coefficient matrix to the vector state **x** clearly shows the periodic states as oscillating variables; note the submatrices in the lower quadrant. These periodics are added to the phase state in the second row and then, by extension, are incorporated in the second phase state. Since the harmonics are integrated into the system, rather than added at each epoch, there is no epoch dependent $\mathbf{M}_k$ matrix for this model. The pre–process noise multiplier is unchanged for this model since the incorporation of noise to the second phase state is the same. Hence, $\mathbf{G}_{\mathrm{II}} = \mathbf{G}_{\mathrm{I}}$. The discrete propagation model will be

$$\mathbf{x}_{k+1} = \Phi_{\mathrm{II}}\mathbf{x}_k + \mathbf{G}_{\mathrm{II}}\mathbf{s}_k$$

where

$$\Phi_{\mathrm{II}} = \begin{bmatrix}
0 & 1 & \tau & \tau^2/2 & \frac{\sin(\nu_1\tau)}{\nu_1} & \frac{1-\cos(\nu_1\tau)}{\nu_1} & \frac{\sin(\nu_2\tau)}{\nu_2} & \frac{1-\cos(\nu_2\tau)}{\nu_2}\\
 & 1 & \tau & \tau^2/2 & \frac{\sin(\nu_1\tau)}{\nu_1} & \frac{1-\cos(\nu_1\tau)}{\nu_1} & \frac{\sin(\nu_2\tau)}{\nu_2} & \frac{1-\cos(\nu_2\tau)}{\nu_2}\\
 & & 1 & \tau & & & & \\
 & & & 1 & & & & \\
 & & & & \cos(\nu_1\tau) & \sin(\nu_1\tau) & & \\
 & & & & -\sin(\nu_1\tau) & \cos(\nu_1\tau) & & \\
 & & & & & & \cos(\nu_2\tau) & \sin(\nu_2\tau)\\
 & & & & & & -\sin(\nu_2\tau) & \cos(\nu_2\tau)
\end{bmatrix}.$$

As in the previous model, the covariance matrix is obtained by multiple integration of $\Phi$ and **S** with a delta

function. Equation (4) can be used to obtain $E\left[\mathbf{G}_{\mathrm{II}}\mathbf{s}_k\,\mathbf{s}_k^T\,\mathbf{G}_{\mathrm{II}}^T\right] = \mathbf{G}_{\mathrm{II}}(\mathbf{Q}_L + \mathbf{Q}_L^T)\mathbf{G}_{\mathrm{II}}^T$ where

$$\mathbf{Q}_L = \begin{bmatrix} S_1\frac{f_h}{2} & 0 & 0 & 0 & 0 & 0 & 0 & 0 \\ 0 & S_2\frac{\tau}{2} + S_3\frac{\tau^3}{6} + S_4\frac{\tau^5}{40} + S_h\Omega & 0 & 0 & 0 & 0 & 0 & 0 \\ 0 & S_3\frac{\tau^2}{2} + S_4\frac{\tau^4}{8} & S_3\frac{\tau}{2} + S_4\frac{\tau^3}{6} & 0 & 0 & 0 & 0 & 0 \\ 0 & S_4\frac{\tau^3}{6} & S_4\frac{\tau^2}{2} & S_4\frac{\tau}{2} & 0 & 0 & 0 & 0 \\ 0 & -S_h\frac{\cos(\nu_1\tau)}{\nu_1^2} & 0 & 0 & S_h\frac{\tau}{2} & 0 & 0 & 0 \\ 0 & S_h\frac{\sin(\nu_1\tau)-\nu_1\tau}{\nu_1^2} & 0 & 0 & 0 & S_h\frac{\tau}{2} & 0 & 0 \\ 0 & -S_h\frac{\cos(\nu_2\tau)}{\nu_2^2} & 0 & 0 & 0 & 0 & S_h\frac{\tau}{2} & 0 \\ 0 & S_h\frac{\sin(\nu_2\tau)-\nu_2\tau}{\nu_2^2} & 0 & 0 & 0 & 0 & 0 & S_h\frac{\tau}{2} \end{bmatrix}$$

and

$$\Omega = \frac{\nu_1\tau - \sin(\nu_1\tau)}{\nu_1^3} + \frac{\nu_2\tau - \sin(\nu_2\tau)}{\nu_2^3}.$$

### Model III

In the third and final model, the harmonic states are again treated as oscillating variables. This model is distinct from Model II since the harmonic variables are coupled directly to the drift state rather than only the phase state. From the diagram in Figure 3, one can see that the harmonic states (along with their white noise components) will be integrated three times. The impact of these states on the phase will therefore be significantly more complex. This is expected given that successive integrations from the drift state yield

$$x_1(t) = u_1(t) + \int^t \left[u_2(s) + \int^s \left(u_3(\xi) + \int^\xi \left(u_4(\eta) + x_5(\eta) + x_7(\eta)\right) d\eta\right) d\xi\right] ds.$$

The continuous differential model for the entire system is again of the form in Equation (1). As in Models I and II, we have $\mathbf{C}_{\mathrm{III}} = \mathbf{C}_{\mathrm{I}}$ and $\mathbf{G}_{\mathrm{III}} = \mathbf{G}_{\mathrm{I}}$. For Model III, we have the system of differential equations

$$\mathbf{C}_{\mathrm{III}}\frac{d\mathbf{x}}{dt} = \begin{bmatrix} 1 & -1 & 0 & 0 & & & & \\ 0 & 0 & 1 & 0 & & & & \\ 0 & 0 & 0 & 1 & & & & \\ 0 & 0 & 0 & 0 & 1 & 0 & 1 & 0 \\ & & & & 0 & \nu_1 & & \\ & & & & -\nu_1 & 0 & & \\ & & & & & & 0 & \nu_2 \\ & & & & & & -\nu_2 & 0 \end{bmatrix} \mathbf{x}(t) + \mathbf{G}_{\mathrm{III}}\mathbf{u}(t). \tag{9}$$

Notice that the periodic variables are added to the drift state. Since the drift integrates to the frequency which in turn integrates to phase, the periodic effect is propagated through the entirety of the clock states.

The discrete time model is again of the form

$$\mathbf{x}_{k+1} = \Phi_{\mathrm{III}}\mathbf{x}_k + \mathbf{G}_{\mathrm{III}}\mathbf{s}_k$$

where the transition matrix is now

$$\Phi_{\mathrm{III}} = \begin{bmatrix}
0 & 1 & \tau & \tau^2/2 & \frac{\nu_1\tau-\sin(\nu_1\tau)}{\nu_1^3} & \frac{\nu_1^2\tau^2-2+2\cos(\nu_1\tau)}{2\nu_1^3} & \frac{\nu_1\tau-\sin(\nu_2\tau)}{\nu_2^3} & \frac{\nu_2^2\tau^2-2+2\cos(\nu_2\tau)}{2\nu_2^3} \\
 & 1 & \tau & \tau^2/2 & \frac{\nu_1\tau-\sin(\nu_1\tau)}{\nu_1^3} & \frac{\nu_1^2\tau^2-2+2\cos(\nu_1\tau)}{\nu_1^3} & \frac{\nu_1\tau-\sin(\nu_2\tau)}{\nu_2^3} & \frac{\nu_2^2\tau^2-2+2\cos(\nu_2\tau)}{2\nu_2^3} \\
 & & 1 & \tau & \frac{1-\cos(\nu_1\tau)}{\nu_1^2} & \frac{\nu_1\tau-\sin(\nu_1\tau)}{\nu_1^2} & \frac{1-\cos(\nu_2\tau)}{\nu_2^2} & \frac{\nu_2\tau-\sin(\nu_2\tau)}{\nu_2^2} \\
 & & & 1 & \frac{\sin(\nu_1\tau)}{\nu_1} & \frac{1-\cos(\nu_1\tau)}{\nu_1} & \frac{\sin(\nu_2\tau)}{\nu_2} & \frac{1-\cos(\nu_2\tau)}{\nu_2} \\
 & & & & \cos(\nu_1\tau) & \sin(\nu_1\tau) & & \\
 & & & & -\sin(\nu_1\tau) & \cos(\nu_1\tau) & & \\
 & & & & & & \cos(\nu_2\tau) & \sin(\nu_2\tau) \\
 & & & & & & -\sin(\nu_2\tau) & \cos(\nu_2\tau)
\end{bmatrix}.$$

Note that $\Phi_{\mathrm{III}}$ has far lower sparsity than $\Phi_{\mathrm{I}}$. The covariance matrix will not be shown here since some entries of that matrix contain hundreds of terms. One may compute $\mathbf{Q}_k$ using Equation (4), but it is only necessary for the reader to be aware that $\mathbf{Q}_k$ is less sparse and contains substantially more complicated terms.

## CLOCK ENSEMBLE AND KALMAN FILTER PROCESS

An important concern in this report is the number of calculations that must be carried out in order to attain the state vector $\mathbf{x}_k$ from the state vector at the previous time step, $\mathbf{x}_{k-1}$. Given that the actual state vector is unknown, a process that involves updating estimates of the clock is needed. We assume some initial estimate for the state vector, $\widehat{\mathbf{x}}_0$. Then, using the transition matrix $\Phi$, we update the state vector to estimates at the next time step, namely $\widehat{\mathbf{x}}_1$. This propagation follows the base discrete model of Equation (2) without the noise term. Since the noise is random, it can be neither predicted nor applied to the deterministic propagation. As shown in Figure 4, the filter produces a series of clock state estimates, almost surely not equal to the actual clock states. Even the initial condition $\widehat{\mathbf{x}}_0$ is a guess that is not equal to $\mathbf{x}_0$.

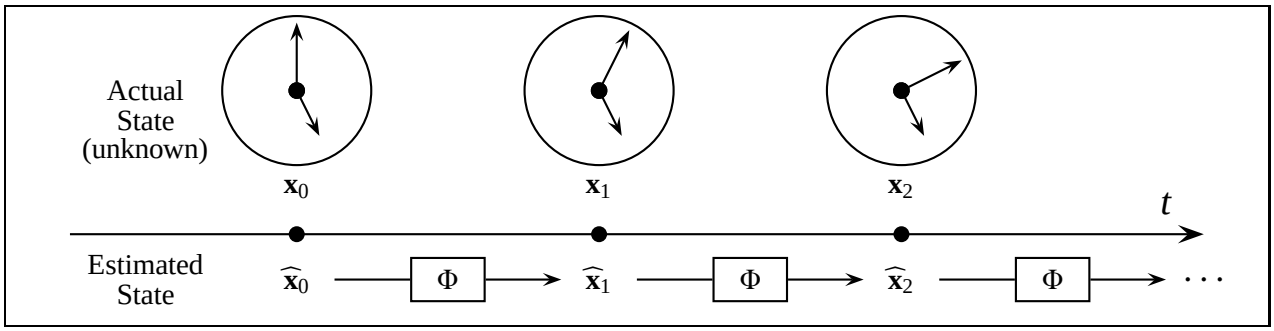


Figure 4. Actual versus estimated clock states.

In order to compare the state of the physical clock to the state estimates, there must be a measurement of the clock's phase. Since a clock may only be observed with respect to another clock, there will be a need for more than one single clock before the notion of measurements and updates can be considered. Before continuing on this front, a model for an ensemble of clocks is presented.

### Ensemble of Clocks

Consider a set of $N$ clocks each of which has four clock states as well as four independent noise inputs. Thus, for clock $i$, we have the four states $x_1^{[i]}, x_2^{[i]}, x_3^{[i]}$ and $x_4^{[i]}$ as well as the noise inputs $u_1^{[i]}, u_2^{[i]}, u_3^{[i]}$ and $u_4^{[i]}$. A GPS clock will also have the additional four periodic states and their associated noise processes. The two phase states of all the clocks are assembled together followed by the frequency states and then the drift states into a single large state vector. The same organization applies to the noise input vector and so one has,

$$\mathbf{x} \;=\; \left[\, x_1^{[1]}, x_1^{[2]}, \cdots, x_1^{[N]}, \;\; x_2^{[1]}, x_2^{[2]}, \cdots, x_2^{[N]}, \cdots, \cdots, \;\; x_8^{[1]}, x_8^{[2]}, \cdots, x_8^{[N]} \,\right]^T$$

and

$$\mathbf{u} \;=\; \left[\, u_1^{[1]}, u_1^{[2]}, \cdots, u_1^{[N]}, \;\; u_2^{[1]}, u_2^{[2]}, \cdots, u_2^{[N]}, \cdots, \cdots, \;\; u_8^{[1]}, u_8^{[2]}, \cdots, u_8^{[N]} \,\right]^T$$

For simplicity, assume all clocks have 8 states where masers and cesium clocks have the periodic states "turned off" by setting them to zero. The system transition matrix is a size $8N$ square matrix and is obtained by the Kronecker product of the base transition matrix $\Phi_\alpha$ with the size $N$ identity. The discrete model for the ensemble therefore becomes

$$\mathbf{x}_{k+1} \;=\; (\Phi_\alpha \otimes \mathbf{I}_N \;+\; \mathbf{1}_{\mathrm{I}}(\alpha)\, \mathbf{M}_k \otimes \mathbf{I}_N)\mathbf{x}_k \;+\; (\mathbf{G}_\alpha \otimes \mathbf{I}_N)\mathbf{s}_k \tag{10}$$

where $\alpha \in \{\mathrm{I}, \mathrm{II}, \mathrm{III}\}$ is the model number and $\mathbf{1}_{\mathrm{I}}(\alpha)$ is the indicator function that returns 1 if $\alpha = \mathrm{I}$ and 0 otherwise. One can expand the matrices defined here to reveal the structure of the transition matrix and process noise pre–multiplier for an ensemble of clocks.

Each clock will have its own independent collection of zero–mean input noises, $u_1^{[i]}, \cdots u_8^{[i]}$, where each of these noises corresponds to the initial definitions of $u_1, \cdots, u_8$, respectively. We may then construct a continuous version of the associated covariance matrix

$$E\left[\, \mathbf{u}(t)\, \mathbf{u}^T(t') \,\right] \;=\; \mathrm{Diag}\Big[\, S_1^{[1]}, S_1^{[2]}, \cdots, S_1^{[N]}, \cdots, \cdots, S_8^{[1]}, S_8^{[2]}, \cdots, S_8^{[N]} \,\Big]\, \delta_0(t - t')$$

where we define the matrix of spectral densities to be $\mathbf{S}$, as usual. The discrete version of the covariance matrix for the ensemble case is obtained as in Equation (4). In particular, one can use

$$\left[(\mathbf{G} \otimes \mathbf{I}_N)\, \mathbf{Q}\, (\mathbf{G} \otimes \mathbf{I}_N)^T\right]_{i,j} \;=\; \int_{t_k}^{t_{k+1}} \left( \sum_{n=1}^{8N} \left[\Phi_\alpha(\xi) \otimes \mathbf{I}_N\right]_{i,n} \left[\, \mathbf{S} \,\right]_{n,n} \left[\Phi_\alpha(\xi) \otimes \mathbf{I}_N\right]_{j,n} \right) d\xi,$$

to obtain $\mathbf{Q}$. Note that since $\Phi_\alpha(\xi) \otimes \mathbf{I}_N$ is quite sparse, many elements of $\mathbf{Q}$ will be zero.

### KALMAN FILTER ESTIMATION PROCESS

With the model for a clock ensemble complete, it remains to detail the manner by which measurements are treated. For an ensemble of $N$ clocks, we fix clock #$N$ as the reference. Hence, all clock phase measurements are observed with respect to clock #$N$. It is these measurements which contribute to the Kalman Filter and update the propagated estimates of the state vector. In order to build an appropriate filter, we must relate the measurements to the state vector. Define the vector

$$\mathbf{z}(t_k) \;=\; \left[\, z^{[1]}(t_k)\,,\; z^{[2]}(t_k)\,,\; z^{[3]}(t_k)\,,\cdots,\; z^{[N-1]}(t_k) \,\right]$$

to be the set of measurements at time $t_k$ where $z^{[i]}(t_k) = x_1^{[i]}(t_k) - x_1^{[N]}(t_k)$ is the observed phase of clock $i$ with respect to the reference clock $N$. We may then relate $\mathbf{x}_k$ and $\mathbf{z}_k$ by the equation

$$\mathbf{z}(t_k) - \mathbf{H}\,\mathbf{x}(t_k) \;=\; \mathbf{0}_{(N-1),1} \tag{11}$$

where the observation matrix is

$$\mathbf{H} \;=\; \begin{bmatrix} 1 & 0 & 0 & \cdots & 0 & -1 & \mathbf{0}_{1,7N} \\ 0 & 1 & 0 & \cdots & 0 & -1 & \mathbf{0}_{1,7N} \\ 0 & 0 & 1 & \cdots & 0 & -1 & \mathbf{0}_{1,7N} \\ \vdots & \vdots & \vdots & \ddots & \vdots & \vdots & \vdots \\ 0 & 0 & 0 & \cdots & 1 & -1 & \mathbf{0}_{1,7N} \end{bmatrix}_{(N-1),8N} .$$

Since the state estimates of the clocks are not equal to the true state values, we will encounter the observation equation in the form

$$\mathbf{z}(t_k) - \mathbf{H}\widehat{\mathbf{x}}(t_k) \;=\; \mathbf{v}(t_k) \tag{12}$$

where $\mathbf{v}$ is the vector of clock residuals. See Figure 5 for a diagram of the Kalman propagation and measurement update routine at epoch $t_k$.

With the discrete plant of Equation (10) and observation Equation (12) specified, a Kalman filter may now be implemented recursively. These standard equations are included here for completeness **[7]**. We are interested in propagating estimates of the combined state and its error covariance from time epoch $t_{k-1}$ to $t_k$. Assume that state estimates and error covariance are given at $t_{k-1}$ respectively as $\widehat{\mathbf{x}}(t_{k-1})$ and $\mathbf{P}(t_{k-1})$. An *a priori* estimate of the state vector can be obtained by

$$\widehat{\mathbf{x}}(t_k^-) \;=\; \Phi\widehat{\mathbf{x}}(t_{k-1}) \tag{13}$$

where $t_k^-$ is used to indicate the *a priori* nature of this estimate; $\widehat{\mathbf{x}}(t_k^-)$ is prior in the sense that it predicts $\widehat{\mathbf{x}}(t_k)$ without any input of the measurement $\mathbf{z}(t_k)$. The error in the *a priori* state vector is defined as

$$\mathbf{e}(t_k^-) \;=\; \mathbf{x}(t_k) - \widehat{\mathbf{x}}(t_k^-)$$

which has the associated *a priori* error covariance matrix $\mathbf{P}(t_k^-) \;=\; E\left[\,\mathbf{e}(t_k^-)\mathbf{e}^T(t_k^-)\,\right]$. The *a priori* error covariance matrix is predicted from $\mathbf{P}(t_{k-1})$ by

$$\mathbf{P}(t_k^-) \;=\; \Phi\mathbf{P}(t_{k-1})\Phi^T + \mathbf{G}\mathbf{Q}(t_{k-1})\mathbf{G}^T. \tag{14}$$

The *a posteriori* estimates are attained by including measurement data. The measurements at $t_k$ are arranged

into a vector along with an accompanying observation matrix of Equation (12). The Kalman gain, state vector and covariance matrix updates are found in the usual way:

$$\mathbf{K}(t_k) = \mathbf{P}(t_k^-)\mathbf{H}^T \left(\mathbf{H}\mathbf{P}(t_k^-)\mathbf{H}^T + \mathbf{R}\right)^{-1}; \tag{15}$$

$$\widehat{\mathbf{x}}(t_k) = \widehat{\mathbf{x}}(t_k^-) + \mathbf{K}\left(\mathbf{z}(t_k) - \mathbf{H}\widehat{\mathbf{x}}(t_k^-)\right); \tag{16}$$

$$\mathbf{P}(t_k) = \mathbf{P}(t_k^-) - \mathbf{K}\mathbf{H}\mathbf{P}(t_k^-). \tag{17}$$

The *a posterior* error covariance can be calculated as shown in Equation (17) but is initially defined as

$$\mathbf{P}(t_k) = E\left[\,\mathbf{e}(t_k)\,\mathbf{e}^T(t_k)\,\right],$$

where the vector of errors is

$$\mathbf{e}(t_k) = \mathbf{x}(t_k) - \widehat{\mathbf{x}}(t_k).$$

The Kalman filter that is employed in this study contains other clock statistic evaluations such as down–weighting, spectral density adaptation, ensemble membership control (based on steady state of clocks), phase break and frequency break detection. These effects are mostly switched off for the tests presented in this paper. The details surrounding these other elements are eliminated here since they are not changed from one model to the next and therefore have little bearing on the GPS model comparison.

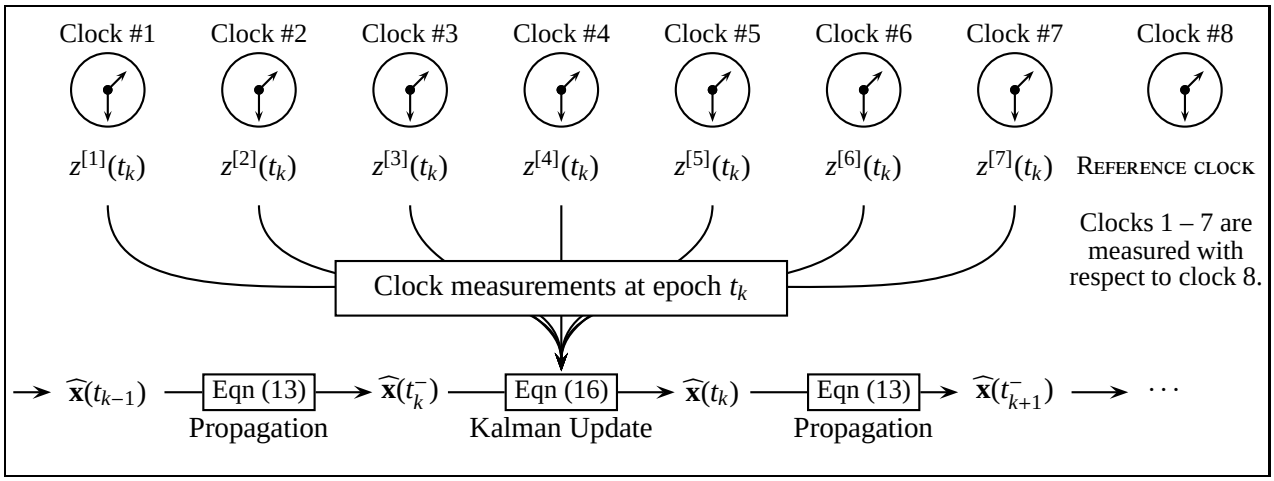


Figure 5. Measurements from an eight clock ensemble being used to update the a priori estimates of the state $\widehat{\mathbf{x}}(t_k^-)$, at epoch $t_k$ to the a posteriori estimates $\widehat{\mathbf{x}}(t_k)$.

## FILTER PERFORMANCE AND RESULTS

In this section, we present results of the filter when equipped with each of the three models discussed earlier. The statistics arising from the estimated clock phase are compared with the statistics of the true clock phase to assess the validity of each model and determine the extent to which each can apply to the filter and generate an accurate timescale. In addition, an analysis of the computation time is presented. Loss of algorithm speed is one concern when using a more complex, yet precise model. Ultimately, a comparison of the accuracy and speed are made to determine the trade–off in selecting a particular modeling approach for the GPS clocks and their periodics.

### COMPUTATIONAL COMPLEXITY

The state and covariance propagation, which take place in Equations (13) and (14), are of primary interest in this report. It is these two computations that involve the transition and noise covariance matrices and hence where the complexity of the model is most relevant. The update step of Equations (15) (16) and (17) are not as relevant since they are not directly dependent on the different models presented earlier. These update equations show how the observation matrix **H** (of constant sparsity) dominates the matrix products.

We can determine the complexity based roughly on the number of clocks with harmonics $N_h$ and the number of clocks without harmonics $N_w$. The number of clocks and presence of additional states are the main factors affecting the size and complexity of $\Phi$ and **Q**. Clocks without harmonics will have entries of zero in the right hand half of the transition matrix. This is important to note because a matrix product can be done faster when the trivial computations are neglected.

Our filter algorithm employs a UD–factorization of the error covariance matrix **P** in order to help speed the algorithm and maintain a symmetric structure in **P**. The routine used to propagate and update the estimates is due to Catherine Thornton and can be found in **[8]**. This routine actually updates the **U** and **D** factors so that

$$\mathbf{U}(t_k)\mathbf{D}(t_k)\mathbf{U}^T(t_k) \;=\; \mathbf{U}(t_{k-1})\mathbf{D}(t_{k-1})\mathbf{U}^T(t_{k-1})\Phi^T + \mathbf{G}\mathbf{Q}(t_{k-1})\mathbf{G}^T.$$

The formulas in Table 1 show (roughly) the number of numerical products that must be made in order to propagate the state and covariance in the Kalman Filter. Note that the number needed is more than twice as great for Model III versus Model I.

Table 1. Comparison of calculations required at the propagation step.

| Model | Number of Calculations | | $N_h = 24$ and $N_w = 17$ | |
|---|---|---|---|---|
| Number | $\Phi\widehat{\mathbf{x}}$ | $\Phi\mathbf{U}$ | Total | Ratio versus Model I |
| I | $15N_h + 7N_w$ | $368N_h^2 + 316N_wN_h + 60N_w^2$ | 296,651 | 1.00 |
| II | $19N_h + 7N_w$ | $600N_h^2 + 524N_wN_h + 108N_w^2$ | 492,677 | 1.66 |
| III | $27N_h + 7N_w$ | $952N_h^2 + 796N_wN_h + 164N_w^2$ | 766,475 | 2.58 |

NB: Formulas are approximate to simplify exposition.

### TIMESCALE STATISTICS AND FILTER TESTS

The following statistics are based on estimates of the clocks and associated timescales from our filter. We present both the computation time and the variance statistics of the timescales for each of the three models. Input parameters for the spectral densities and GPS clock periodics are shown below in Table 2.

These input parameters are needed to generate a data set for the 41 clocks. Each clock is simulated for a period of 100 days with discrete time epochs spaced at $\tau = 300$ seconds (5 minutes). The simulations produce true states for all the clocks $\mathbf{x}(t_k)$ and generate measurements $\mathbf{z}(t_k)$ according to Equation (11). These measurements are passed to the filter three times (each pass with a different GPS clock model) for testing.

Table 2. Model parameters assumed for various clock types.

| Clock Class | Cesium | GPS III | USNO Maser | AMC Maser |
|---|---|---|---|---|
| Clock Numbers | 1 – 15 | 16 – 39 | 40 | 41* |
| **Spectral Densities** | | | | |
| $S_1$ ($\text{sec}^2$) | $1.00 \times 10^{-26}$ | $1.00 \times 10^{-26}$ | $1.00 \times 10^{-26}$ | $1.00 \times 10^{-26}$ |
| $S_2$ ($\text{sec}^2/\text{sec}$) | $7.23 \times 10^{-23}$ | $4.90 \times 10^{-23}$ | $1.00 \times 10^{-24}$ | $2.25 \times 10^{-24}$ |
| $S_3$ ($\text{sec}^2/\text{sec}^3$) | $1.00 \times 10^{-38}$ | $1.00 \times 10^{-38}$ | $1.00 \times 10^{-38}$ | $1.00 \times 10^{-38}$ |
| $S_4$ ($\text{sec}^2/\text{sec}^5$) | $1.00 \times 10^{-50}$ | $1.00 \times 10^{-48}$ | $1.00 \times 10^{-50}$ | $1.00 \times 10^{-50}$ |
| **Periodic Frequencies** | | | | |
| $\omega_1$ (cycles/day) | ——— | 2.003 | ——— | ——— |
| $\omega_2$ (cycles/day) | ——— | 4.006 | ——— | ——— |
| **Periodic Amplitude and Phase** | | | | |
| $A_1$ (nsec) | ——— | 0.700 | ——— | ——— |
| $A_2$ (nsec) | ——— | 0.700 | ——— | ——— |
| $\phi_1$ (radians) | ——— | 0 | ——— | ——— |
| $\phi_2$ (radians) | ——— | 0 | ——— | ——— |

*AMC Maser (clock #41) is the reference clock.

The filter processes the measurements using the same spectral density values as defined in Table 2. Estimates of the clock states $\widehat{\mathbf{x}}(t_k)$ are calculated at each time epoch. As the filter processes the batch of measurements, it computes an ensemble clock (weighted average of the 41 clocks being processed). This ensemble clock is the timescale and its estimates along with $\widehat{\mathbf{x}}(t_k)$ are used to calculate Hadamard deviations. The Hadamard deviation of clock #*n* is defined by

$$\widehat{\sigma}_{\alpha}^{[n]}(\tau) \;=\; \sum_{k=1}^{N_T-1} \frac{\widehat{x}_1^{[n]}(t_{k+1}) - 2\widehat{x}_2^{[n]}(t_k) + \widehat{x}_1^{[n]}(t_{k-1})}{6\,(N_k - 2)}$$

where $N_T$ is the total number of epochs for the period of 100 days with $\tau$ as the nominal sampling interval **[9]**. Here, $\alpha \in \{\text{I}, \text{II}, \text{III}\}$ is the model number from which the estimates have been obtained.

In order to simplify the presentation of results and also focus on the filter's performance with respect to the different clock types, Hadamard deviations are averaged over each class of clock. For the ground cesium

clocks, GPS clocks and masers, we compute the average statistics

$$\widehat{\sigma}_\alpha^{\mathrm{C}}(\tau) = \frac{1}{15}\sum_{n=1}^{15}\widehat{\sigma}_\alpha^{[n]}(\tau) \quad , \quad \widehat{\sigma}_\alpha^{\mathrm{G}}(\tau) = \frac{1}{24}\sum_{n=16}^{39}\widehat{\sigma}_\alpha^{[n]}(\tau) \quad , \quad \widehat{\sigma}_\alpha^{\mathrm{M}}(\tau) = \frac{1}{2}\sum_{n=40}^{41}\widehat{\sigma}_\alpha^{[n]}(\tau)$$

respectively. The plots of the deviations are smoothed by these averages since some of the random noise generation is averaged. In Figure 6, the average Hadamard deviation for the different clock types is plotted for the clock estimates of Model I. Note that the deviation of the timescale is also plotted.

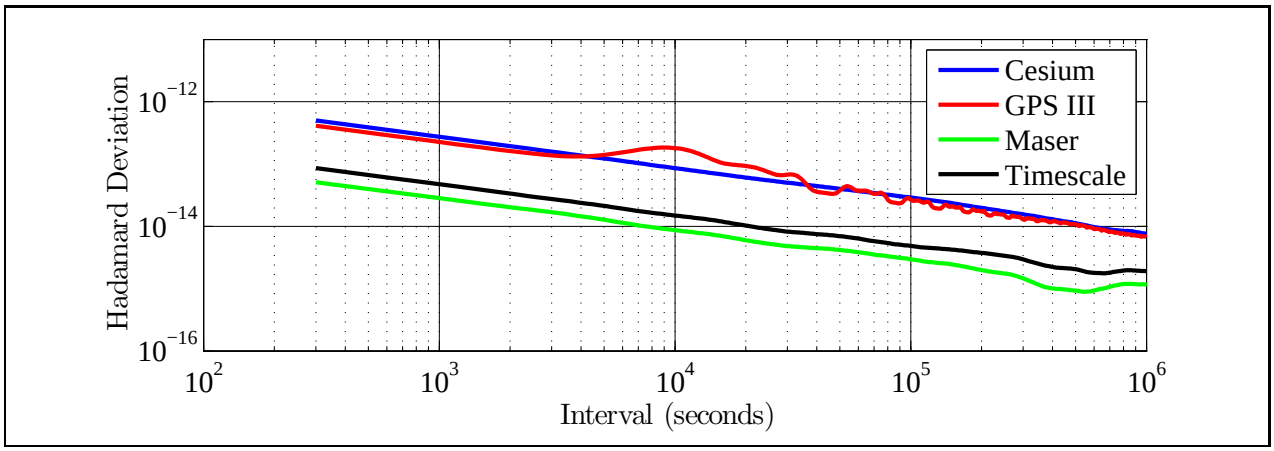


Figure 6. Hadamard deviation plot of clock estimates for Model I.

Recall that the periodic states of Model I were roughly constant weights of the deterministic functions $\cos(2\pi\omega t)$ and $\sin(2\pi\omega t)$. This differs substantially from the Model II version where the periodic states were sinusoidal states themselves and then superimposed on the phase states of the clock. Despite this difference, the filter extracts similar deviation statistics when using either of these models. Figure 7 shows the difference between the Hadamard deviation plots of Models I and II. Note these differences are less in magnitude in comparison to the plotted timescale of Model I. The cause of the sinusoidal difference is likely the decorrelation (Model I) versus correlation (Model II) of the periodic and clock states.

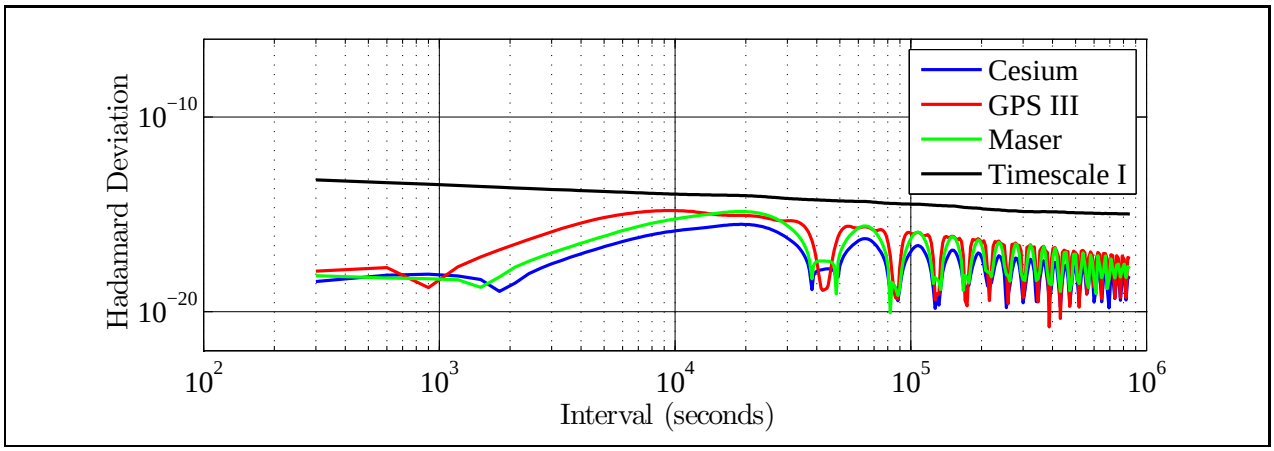


Figure 7. Differences between the Hadmard deviations of the Model I and Model II estimates of each clock type. These are plotted along side the Hadamard deviation of Timescale I showing that all Model differences are below the timescale performance.

In Figure 8, the deviations of all three timescales are plotted. The timescales resulting from the different models are remarkably similar. It is important to note, however, that the Model III timescale is based on predicted clock values. The actual clock estimates for Model III yield a poorer performing timescale. Extensive experimentation with the third model has suggested that even small amounts of noise at the drift level can amplify upon integration and have great effects on the clock phase estimates. Such is likely the case in Model III since the periodic states are integrated from the level of drift. There are hypothesis for this behavior, but these inaccuracies are not an issue or a central problem here. The difference in the deviation of the timescale from Model I to the true output of Model III is sufficiently low to suggest that Models I and II are able to produce reasonably accurate timescales.

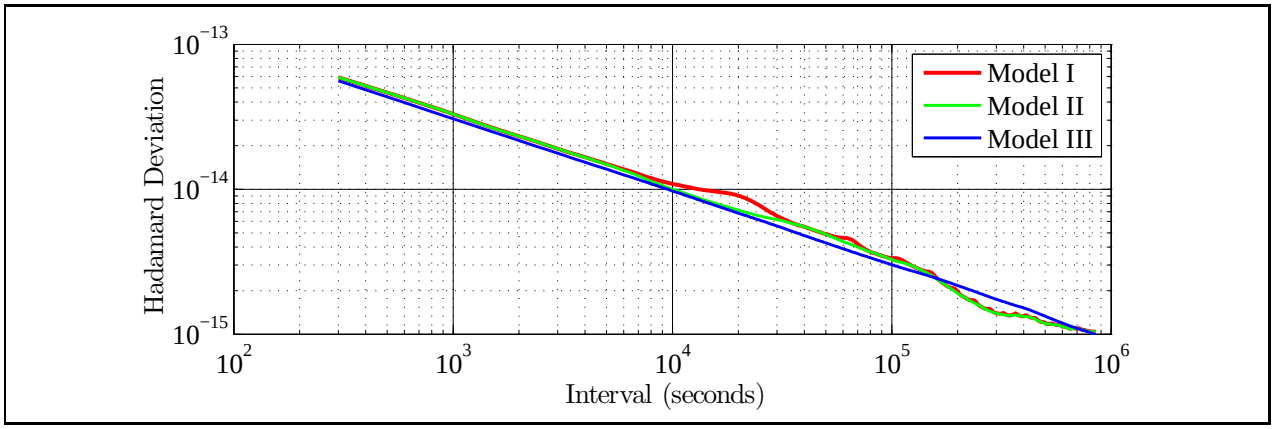


Figure 8. Comparison of timescales for Models I, II (estimates) and III (predicted).

In order to compare the models, we measure the absolute difference between the averaged Hadamard deviations of the estimates and true clock values. An average of these differences over $\tau$ then gives a measure of the model's performance for each clock class. Define the average difference between the Hadamard deviation of the model's estimate and true states to be

$$\Delta_\alpha^C = \frac{1}{|T|} \sum_{\tau \in T} \left| \widehat{\sigma}_\alpha^C(\tau) - \sigma^C(\tau) \right|$$

where $T$ is the set of epochs over which the filter was run. Table 3 contains numerical results of this measure. Note that the average difference of the deviations are relatively best for Model II while Model III performs poorest. This is consistent with the analysis of the timescales earlier. In Figure 8, one can note that the Model I timescale contains greater influence from the periodic states. The Model II timescale has less variation by comparison. This may advocate for correlating the periodic states to the clock phase, but not fully correlating and coupling the entire clock.

In Table 3, results of the filter speed are also presented. The variable $p_\alpha$ is the computation time in seconds per epoch when model $\alpha$ is employed. The effects of the propagation step are evident by the ratio of time needed with respect to Model I. The ratios compare well with the ratios of Table 1. They are expectedly less pronounced in Table 3 since an entire epoch of computations includes calculations outside of the propagation step where the models' differences are less relevant to computation time.

Table 3. Model comparisons. Left side: Average difference between true and estimated clock statistics over the full range of $\tau$. Right side: Comparison of algorithm speed.

| Model | Deviation Comparisons | | | Speed Comparisons | |
|---|---|---|---|---|---|
| $\alpha$ | $\Delta_\alpha^{\mathrm{C}}$ | $\Delta_\alpha^{\mathrm{G}}$ | $\Delta_\alpha^{\mathrm{M}}$ | $p_\alpha$ | $p_\alpha / p_{\mathrm{I}}$ |
| I | $2.86 \times 10^{-16}$ | $4.70 \times 10^{-16}$ | $1.33 \times 10^{-15}$ | 0.0722 sec | 1.0000 |
| II | $3.34 \times 10^{-16}$ | $3.05 \times 10^{-16}$ | $1.12 \times 10^{-15}$ | 0.0790 sec | 1.0943 |
| III | $1.15 \times 10^{-15}$ | $8.29 \times 10^{-16}$ | $3.87 \times 10^{-15}$ | 0.1584 sec | 2.1932 |

## CONCLUSIONS

Simplified GPS clock models that partially decorrelate the harmonic states from the clock states do not severely compromise the accuracy of the filter or performance of the timescale. These results have demonstrated, however, that simpler models can decrease the computation complexity and hence processing time of the filter algorithm.

The model which fully couples the harmonics states to the clock states is highly complex with several noise components that are added to the drift state. Since the drift is integrated twice before affecting the clock phase, the periodic states and their corresponding noises profoundly disturb the model's phase output. Such complications are unnecessary for accuracy and actually hinder accurate filtering of the clock phase.

Although there are considerable speed improvements for the decorrelated model, the second model seems to offer a reasonably fast alternative. The primary difference with Model II is that the phase states are stochastically correlated to the periodic states. There were noticeable accuracy improvements for this filter without too much additional computational complexity. It may be beneficial to consider such a model or a variant as a reasonable trade–off between complexity and accuracy.

## REFERENCES

**[1]** K. Senior, J. Ray and R.L. Beard, 2008, "*Characterization of periodic variations in the GPS satellite clocks*," **GPS Solutions**, **Volume 12**, 211–225.

**[2]** R.G. Brown, P.Y.C. Hwang, 1997, **Introduction to Random Signals and Applied Kalman Filtering, 3rd Edition**, (John Wiley and Sons, New York).

**[3]** R.H. Jones and P.V. Tryon, 1983, "*Estimating time from atomic clocks*," **Journal of Research of the National Bureau of Standards**, **Volume 88**, 17–24.

**[4]** P.V. Tryon and R.H. Jones, 1983, "*Estimation of parameters in models for cesium beam atomic clocks*," **Journal of Research of the National Bureau of Standards**, **Volume 88**, 3–16.

**[5]** S.R. Stein, 1989, "*Kalman filter analysis of precision clocks with real–time parameter estimation*," **Proceedings of the 43rd Annual Symposium on Frequency Control**, Denver, Colorado, pp. 232–236.

**[6]** S.T. Hutsell, 1995, "*Relating the Hadamard variance to MCS kalman filter clock estimation*," **Proceedings of the 27th Annual Precise Time and Time Interval (PTTI) Applications and Planning Meeting**, San Diego, California, pp. 291–302.

**[7]** P.S. Maybeck, 1979, **Stochastic Models, Estimation and Control, Volume 1**, (Academic Press, New York).

**[8]** M.S. Grewal, 2001, **Kalman Filtering: Theory and Practice Using MATLAB, 2nd Edition**, (John Wiley and Sons, New York).

**[9]** S.T. Hutsell, W.G. Reid, 1Lt J.D. Crum, 1Lt H.S. Mobbs, J.A. Buisson, 1996, "*Operational use of the Hadamard variance in GPS*," **Proceedings of the 28th Annual Precise Time and Time Interval (PTTI) Applications and Planning Meeting**, Reston, Virginia, pp. 201–214.